AFRL-RV-HA-TR-2007-1134

Ionospheric Modeling: Development, Verification and Validation

Patricia H. Doherty
Leo F. McNamara
William J. Burke
William J. McNeil
Louise C. Gentile

Boston College
Institute for Scientific Research
140 Commonwealth Avenue
Chestnut Hill, MA 02467-3862

Scientific Report No. 3

15 August 2007

AIR FORCE RESEARCH LABORATORY
Space Vehicles Directorate
29 Randolph Road
AIR FORCE MATERIEL COMMAND
Hanscom AFB, MA 01731-3010

Report Documentation Page

Form Approved
OMB No. 0704-0188

1. REPORT DATE	2. REPORT TYPE	3. DATES COVERED
15 AUG 2007		

4. TITLE AND SUBTITLE	5a. CONTRACT NUMBER
Ionospheric Modeling: Development, Verification and Validation	**FA8718-04-C-0055**
	5b. GRANT NUMBER
	5c. PROGRAM ELEMENT NUMBER **62601F**

6. AUTHOR(S)	5d. PROJECT NUMBER
Patricia Doherty; Leo McNamara; William Burke; Louise Gentile	**1010**
	5e. TASK NUMBER **SD**
	5f. WORK UNIT NUMBER **A1**

7. PERFORMING ORGANIZATION NAME(S) AND ADDRESS(ES)	8. PERFORMING ORGANIZATION REPORT NUMBER
Boston College,Institute for Scientific Research,140 commonwealth Avenue,Chestnut Hill,MA,02467	

9. SPONSORING/MONITORING AGENCY NAME(S) AND ADDRESS(ES)	10. SPONSOR/MONITOR'S ACRONYM(S)
	11. SPONSOR/MONITOR'S REPORT NUMBER(S)

12. DISTRIBUTION/AVAILABILITY STATEMENT

Approved for public release; distribution unlimited.

13. SUPPLEMENTARY NOTES

14. ABSTRACT

The objectives of this contract are to improve specification and forcast models currentlyt in use and in development at AFRL. These efforts include performing independent research to augment AFRL's programs in the areas of direct simulation Monte Carlo modeling of chemical releases, Geospace plasma dynamics, validating the theoretical models and applications that are the basis of the Parameterized Real-Time Ionospheric Specification Model (PRISM) and the Inoospheric Forecast Model, and validating the first of the Global Ionospheric Assimilation Models (GAIM). In the past year, we have continued our efforts to calibrate and validate the data products of the SSUSI UV imager on the DMSP F17 satellite. We have also continued a thorough validation of the GAIM model and the WideBand Sciontillation Model (WBMod). In addition,we have initiated studies of Magnetosphere-Ionosphere-Thermosphere coupled models.

15. SUBJECT TERMS

16. SECURITY CLASSIFICATION OF:			17. LIMITATION OF ABSTRACT	18. NUMBER OF PAGES	19a. NAME OF RESPONSIBLE PERSON
a. REPORT **unclassified**	b. ABSTRACT **unclassified**	c. THIS PAGE **unclassified**		**30**	

NOTICE AND SIGNATURE PAGE

Using Government drawings, specifications, or other data included in this document for any purpose other than Government procurement does not in any way obligate the U.S. Government. The fact that the Government formulated or supplied the drawings, specifications, or other data does not license the holder or any other person or corporation; or convey any rights or permission to manufacture, use, or sell any patented invention that may relate to them.

This report was cleared for public release and is available to the general public, including foreign nationals. Qualified requestors may obtain additional copies from the Defense Technical Information Center (DTIC) (http://www.dtic.mil). All others should apply to the National Technical Information Service.

AFRL-RV-HA-TR-2007-1134 HAS BEEN REVIEWED AND IS APPROVED FOR PUBLICATION IN ACCORDANCE WITH ASSIGNED DISTRIBUTION STATEMENT.

//Signature//	//Signature//
JOHN RETTERER Contract Manager	JOEL MOZER, Chief Space Weather Center of Excellence

This report is published in the interest of scientific and technical information exchange, and its publication does not constitute the Government's approval or disapproval of its ideas or findings.

Table of Contents

Figures

1. EXECUTIVE SUMMARY

During the period August 2006 through July 2007, we continued to pursue the development, verification and validation of ionospheric models in use at AFRL/VSBX. Considerable efforts were made to define calibration algorithms for the data products generated by the Special Sensor Ultraviolet Spectrographic Imager (SSUSI) onboard the Defense Meteorological Satellite Program (DMSP) F17. Further efforts included initial validation of the SSUSI data products. Studies were also performed to validate the Global Assimilation of Ionospheric Measurements (GAIM) models designed by Utah State University and the Jet Propulsion Laboratory. These validation studies focused on the accuracy of GAIM forecasts on TEC and foF2. The benefit of these model validation studies is that they have been used to define modifications for updated versions of the models. Efforts were also continued to assess the abilities of the WideBand Scintillation Model (WBMod) and to determine the benefits of using Global Positioning System scintillation data to improve the model forecasts at L-band frequencies. Studies were also initiated to improve and utilize models of magnetosphere-ionosphere-thermosphere coupling. These studies centered on goals to update the Hardy Auroral model, improve the Satellite Drag Prediction Model and simulate the coupled systems to examine the response of the systems to a variety of changes.

The work summarized above resulted in numerous presentations, twelve published papers in peer reviewed journals and thirteen internal reports.

2. CALIBRATION AND VALIDATION OF DMSP SSUSI IONOSPHERIC SENSORS

Boston College researchers have worked to CALibrate and VALidate (CAL/VAL) the data products generated by the Special Sensor Ultraviolet Spectrographic Imager (SSUSI) that was launched on the Defense Meteorological Satellite Program (DMSP) F17 satellite in September 2006. These efforts included developing a new method to provide absolute calibration of the AFRL SSJ4 and SSJ5 particle detectors; an independent test of the algorithm that calculates the E-layer height and density from the SSUSI observed radiances and initial validations of the data products produced by the SSUSI instrument onboard the DMSP F17 satellite.

2.1. J4 and J5 Precipitation Particle Spectrometer Calibration

Although the pre-flight calibration of the SSJ5 sensor is done as carefully as possible in a vacuum chamber before flight, it does not account for the on-orbit degradation of the channeltron detectors. Channeltrons are susceptible to degradation in performance at the input and output surface. Repeated impacts at these surfaces lessen the secondary emission coefficient of the surface leading to reduced instrument sensitivity. MeV particles in the South Atlantic Anomaly (SAA) are capable of penetrating the sides of the instrument case and triggering the channeltron detectors. The SAA is a relatively stable source of particles that exhibits almost no variation in flux except with respect to the 11-year solar cycle. Precipitating energetic particle fluxes at the low latitudes of the South Atlantic anomaly vary out of phase with the 11-year solar

cycle. Peak fluxes occur during solar minimum. Using the daily average count rate while the instrument is traveling through the South Atlantic anomaly, the degradation of the instrument count rate can be determined.

2.2. Validation of the E-layer Height and Density Algorithm

This CAL/VAL activity involves validation of the mean energy (Eo) and energy flux (Q) of precipitating electrons. Maps of these quantities are found from the SSUSI images as functions of the intensities, and ratios of intensities, of the emissions in the LBH short and long bands. Knowing the characteristics of the precipitating electrons one can calculate the amount of ionization in the E layer. The height of the peak density in the E layer (HmE) and its magnitude (NmE) are additional data products to be supplied by SSUSI. To validate these, we plan to compare the height integrated Pedersen conductivities represented by these E layer densities with the conductivity obtained by and analysis of electric field and magnetic perturbations measured on the satellite.

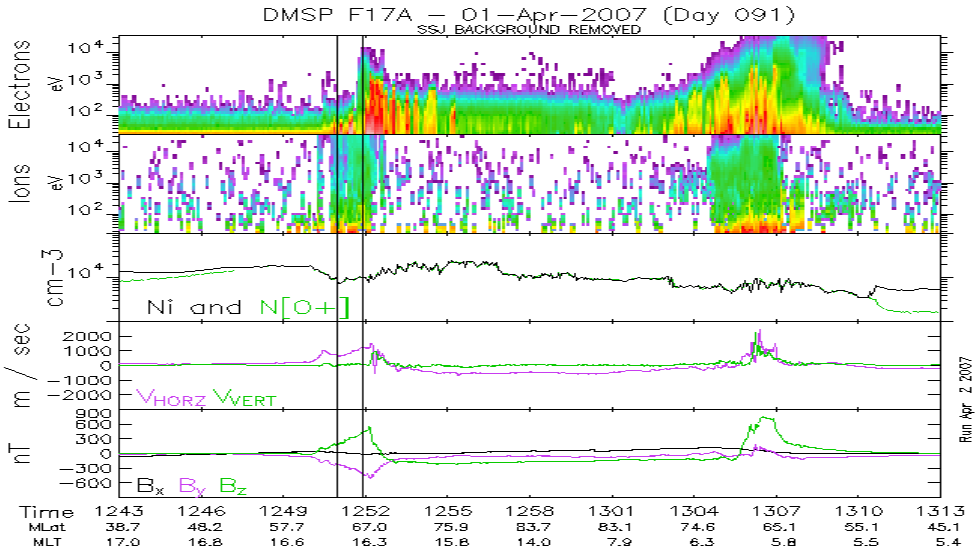

Figure 1. DMSP F17A – 01-Apr-2007 (Day 091). The interval between the two vertical lines is where E_Y and dB_Z have a correlation coefficient of 0.97. As can be seen the primary precipitation is ions and the conductivity in this region is 7.3 mho.

The essence of this technique is that of measuring the voltage across a resistor and the current flowing through it to determine its resistance. In our case, the current is found from the magnetic perturbations measured by the magnetometer on F17 and the electric field comes from the frozen in assumption ($\mathbf{E} = \mathbf{V} \times \mathbf{B}$) which allows us to used the measured plasma drifts as a measure of the electric field. In practice, this approach only works when we can identify an interval in the data where the y component of the electric field and the z component of the magnetic perturbation are highly correlated and linearly related to each other. One such interval is identified in Figure 1. For such intervals, the height integrated Pedersen conductivity is given by $(1/\mu o)\Delta dB_Z/\Delta E_Y$. Currently, we have

identified about 150 such intervals for 6 days of data in April 2007 where activity is high enough that the SSUSI instrument has good data.

One complication to the application of this technique to F17 is the fact that the F17 orbit is primarily dawn – dusk, so that for many of the identified intervals, the solar zenith angle of the E layer under the satellite is less than 90°. For such intervals, solar EUV will make a significant contribution to the conductivities. Fortunately, for these passes, the conductivity is high outside of the auroral oval so that there are often large currents and electric fields that "spill" out of the aurora to low latitudes or into the polar cap. These allow us to find the conductivity in regions with no precipitation that can be used to subtract the solar conductivity contribution from regions with precipitation.

2.3. Initial Validations of SSUSI Measurements from DMSP F17

A comprehensive calibration and validation effort was initiated on the data products provided by the SSUSI sensor on DMSP F17.

One such product is the identification of the equatorward edge of the auroral oval. Figure 2 shows an auroral image from a single F17 northern hemisphere pass on April 1, 2007. The location of the auroral boundary is determined, within the image, by the point where the energy flux drops below 0.2 ergs/cm^2/s. Four red dots in the image indicate locations where equatorward auroral boundaries were identified in the J5 electron precipitation data from F15, F16, and F17, at times close to the middle time of this image (1440 UT). There is apparent good agreement for this case. We are currently in the process of evaluating many more passes to see if the agreement holds up statistically. If not, the plan is to develop means for correcting the SSUSI boundaries to be consistent with the J5 boundaries along the spacecraft ground track and use that relationship to correct the boundaries off track.

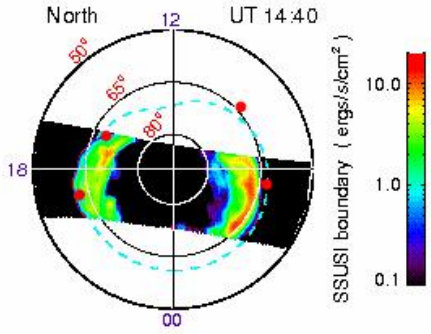

Figure 2. F17 SSUSI auroral image from 1 April 2007. Red dots indicate auroral boundaries found from J5 particle data on F15, F16 and F17.

3. GAIM VALIDATIONS

Numerous GAIM validation efforts have ensued throughout the current year. The most mature studies have been reported in three papers that were published in peer reviewed journals. These papers are listed in the Publications Section of this report. In addition to these publications, twelve internal reports were written to document and summarize the details of our work. These reports were submitted to AFRL and are

available by request from the Institute for Scientific Research at Boston College and Dr. Leo McNamara. The reports are listed below.

Title of Report	File Name	Date
Validation of the GAIM Topside Profiles	GAIM_Topside.book.pdf	Aug 06
Features of the USU-GAIM TEC Assimilation Procedures	GAIM_Assim.book.pdf	Aug06-Jan07
Raytracing Calculations of the Spatial Path Loss for HF Propagation	pathloss.book.pdf	Oct 06
Ionospheric Simulations for Studies of the Single Station Location Technique	SSL_Study.book	Jul-Oct 06
Passive SSL - Using Observations of Check Targets to derive SSL Range Estimates	Check_Target.book.pdf	Nov 06
Investigation of the Reliability of the ESIR Ionogram Autoscaling Method (Expert System for Ionogram Reduction)	ESIR.book.pdf	Dec 06
Quality Figures and Error Bars for Autoscaled Vertical Incidence Ionograms. Background and User Documentation for QualScan V2007.2	AFRL_QualScan.book.pdf	Feb 07
Investigation of the Accuracy of GAIM Forecast Values of foF2 and TEC	GAIM_Forecast.book.pdf	Feb 07
Accuracy of USU-GAIM Values of foF2 and M(3000)F2 for a World-Wide Distribution of Ionosonde Locations	GAIM_WW.book.pdf	Mar 07
Validation of foF2 and M(3000)F2 Specifications Provided by GAIM Models of the Ionosphere	USU_JPL_GAIM.book.pdf	Mar 07
Accuracy of USC/JPL-GAIM Values of foF2 and M(3000)F2 for a World-Wide Distribution of Ionosonde Locations	USC_WW.book.pdf	Apr 07
Differences between USU-GAIM V2.3.1p1 and V2.4.3p1 Values of foF2 and M(3000)F2 for a World-Wide Distribution of Ionosonde Locations	USU_old_new.book.pdf	Jul 07
Validation of QualScan when applied to Ionograms scaled by ARTIST 5	A5V.book.pdf	Jul 07

Further discussion on several of the most comprehensive reports is included in the following sections.

3.1. GAIM_Forecast.book.pdf

This is a 72-page report of a study that investigated the accuracy of GAIM forecasts of foF2 and TEC. The following paragraph is part of the Executive Summary. Version V2.3 of the Utah State University GAIM model has been run for the period 080 through 105 (March/April) 2004, and the forecasts saved for lead times of 1, 2, 3, 6 and 12 hours. The input data include the TEC data for 36 JPL stations along with the DMSP and SAO data (ionosonde profiles), as supplied by USU in its GAIM validation package. The Ionospheric Forecast Model (IFM), Background (BAK), Gauss Markov (GMF; the specification or nowcast) and the five sets of forecast values of foF2 have been compared at ten Australian ionosonde stations and Jicamarca, Peru. All values of foF2 were manually scaled from the ionograms. Forecasts of vTEC have also been compared at five Australian GPS TEC stations (Darwin, Townsville, Tidbinbilla/Canberra, Perth, and Hobart). The GAIM values of each parameter are derived by bilinear interpolation among the four surrounding gridpoints. Because of disk space issues, only the hourly profiles

and key parameters have been used. This is consistent with the cadence of the forecasts. RMS percentage errors in foF2 (and NmF2) and vTEC have been determined, as a way to normalize their large diurnal variations. These errors have been accumulated separately over days and over days/hours. The percentage errors have also been separated into day and night. The errors accumulated over days/hours provide a convenient single error metric for each station. Improvement Ratios have been defined, giving the ratio of the RMS errors for BAK/IFM, and for GMF/BAK. High values of the BAK/IFM ratio indicate that the IFM was already quite accurate, and that improvements over it would be difficult to achieve. Low values of the GMF/BAK ratio indicate a substantial improvement over BAK resulting from the assimilation of the latest real-time data. RMS errors in vTEC have also been calculated for thirty JPL stations distributed world-wide. These stations provided large amounts of TEC observations.

3.2. GAIM_WW.book.pdf

This study investigated the Accuracy of USU-GAIM Values of foF2 and M(3000)F2 for a World-Wide Distribution of 21 Ionosonde Locations. It was found that the USU GAIM had problems over South Africa during the night in September 2006. In response to our findings, USU has modified their code. Further efforts will continue to reevaluate the results of the updated code.

3.3. USU_JPL_GAIM.book.pdf

This study investigated the Accuracy of foF2 and M(3000)F2 Specifications Provided by the USU and USC/JPL GAIM Models of the Ionosphere. The USC/JPL values of M(3000)F2 were found to have been systematic overestimates that corresponded to a height error of ~60 km. This problem was traced to a coarse vertical height grid (80-km steps at the equator). JPL has recently provided AFRL a version of the code that allows the user to specify the vertical height grid. Efforts are in progress to repeat this investigation with the revised code.

3.4. USU_old_new.book.pdf

An earlier analysis showed that the USU GAIM model gave inaccurate plasma frequency profiles at night, especially for South African stations. The profiles were consistently higher than actual measurements. In response to our reports, USU modified their code. We repeated the validation efforts with the modified code against sets of foF2 and M(3000)F2 data for 21 ionospnde sites. Our findings were that the modified code, V2.4.3p1, gave more accurate M(3000)F2 results than the previous version, V2.3.1p1. The work and results of this validation effort is described in this report.

3.5. A5V.book.pdf

The University of Massachusetts (UMass), Lowell, has introduced a new version of their ionogram autoscaling program ARTIST, Version 5. A very extensive study was performed to ensure that the author's program QualScan could handle the results of

ARTIST 5, and that ARTIST 5 performed well on ionograms from a wide variety of stations and months in 2006.

QualScan proved to be very robust, with no failures at all on ~65-K ionograms. However, some parts of QualScan were modified to handle the solar minimum ionograms, which had not been so extensively tested hitherto. Visual inspection of large numbers of ionograms showed evidence of some poorly scaled ionograms. The report has been sent to UMass. The report includes advice to UMass about the problems encountered. The work is briefly described in the Executive Summary of the report.

4. MAGNETOSPHERE-IONOSPHERE-THERMOSPHERE (MIT) MODELING AND SIMULATIONS

Several studies were performed in the current year that centered on the coupling of the magnetosphere, ionosphere and thermosphere. These studies included research to lead to the ultimate goal of updating the Hardy Auroral Model, exploring radically new, model-based methods to address the problem of satellite-drag prediction and using the Integrated Space Weather Prediction Model code to investigate the steady-state configurations of the magnetosphere for both weakly and strongly driven conditions. Many of our investigations have been published in peer reviewed journals. These papers are listed in the Publications Section of this report.

4.1. Characterizing Auroral Precipitation: Updating the Hardy Model

In the past, statistical studies were the favored method of study in characterizing auroral precipitation. Generally, some average characteristic of the electrons or ions (average energy, integral number flux, integral energy flux) was organized by magnetic latitude (MLat) and local time (LT) as a function of a geomagnetic index such as Kp or the orientation of the interplanetary magnetic field. Although much was gained by these studies, there was an inherent problem with this approach. Each of the many different regions of high latitude precipitation such as the polar cap, boundary layer, cusp, boundary plasma sheet, and central plasma sheet, has distinct characteristics. Since the electron characteristics in the adjoining regions can vary greatly, there may be significant differences in the distributions over which the average is done. This can result from variations in the MLat of the boundary from pass to pass at the same Kp level so that the average for a given bin has contributions from both regions or from actual spatial mixing of the populations in some bins in MLat and MLT due to diffusion or other processes. This study was undertaken to characterize the distinct populations within the distribution using an extensive data set from DMSP spacecraft F7 to F15 flying the SSJ4 particle sensor. More than 631,000,000 data points are used in the study covering a range in latitude from the poles to +/-50°. The eventual goal is to update the Hardy auroral model. A manuscript describing the results is currently in preparation for submission to the Journal of Geophysical Research.

4.2. Satellite Drag Prediction Model

Atmospheric drag varies widely with latitude and local time during magnetic storms. However, orbit-averaged drag varies smoothly and is highly correlated with the time histories of predicted magnetospheric electric fields and the Dst index. The two sources of thermospheric energy are solar ultra violet (UV) radiation to the dayside of Earth and depositions of energetic particle and electromagnetic energy at auroral latitudes. Solar UV sources tend to vary slowly while storm time event are sporadic. Clearly, energy deposited in the auroral oval propagates through heat conduction and convection (winds) to lower latitudes during storms. Thermospheric circulations models currently lack good estimates of storm-time energy inputs at auroral latitudes. For the past year, we have been pursuing empirically based methods using measurements of energetic particle and electromagnetic power inputs from the SSJ5, SSIES, and SSM sensors on DMSP F15, F16, and F17 satellites.

Our researchers have been exploring radically new, model-based methods to address the problem of satellite-drag prediction. This approach uses orbit-averaged mass densities inferred from measurements of the accelerometer on the CHAMP and GRACE satellites to estimate globally averaged exospheric temperatures (T_∞) consistent with the Jacchia, 1977 (J77) model now used by Air Force Space Command for thermospheric modeling. They found that, for altitudes h > 90 km, the J77 atmosphere is specified by unique sets of density-temperature profiles that only depend on assigned values of T_∞. By knowing the density at the altitudes of GRACE and/or CHAMP, one can thus calculate T_∞ and the associated neutral density, composition and temperature profiles

With this information, it becomes possible to calculate the total energy budget of the global thermosphere which we treat as a large system that always remains close to thermodynamic equilibrium. In compliance with the first law of thermodynamics, the energy budget has two main components. The first is the total internal energy of the atmosphere $U = 4\pi \int C_V N T r^2 dr$, where C_V is the heat capacity of the atmosphere, N is the total number of moles of gas and T is the temperature Each of the functions in the integrand is a function of r (= R_E + h), parameterized in J77 by T_∞. The second component is the gravitational potential energy of the system $P = 4\pi M_E G \int \rho(r) r dr$, where M_E and G are the mass of the Earth and the universal gravitational constant; $\rho(r)$ represents the mass density profile specified by J77 for specific values of T_∞. For each T_∞, we have calculated the total energy predicted by J77. With CHAMP/GRACE density estimates of T_∞ we plan to examine the changes in total energy of the thermosphere as it evolves during selected magnetic storms. This approach can be validated through comparisons of its predictions of energy inputs with Poynting flux measurements by DMSP satellites as well as with the predictions of theoretical and empirical models. Thereby, our goal is to provide realistic boundary and initial conditions to drive general circulations models.

4.3. Simulations of the Coupled Solar-Wind-Magnetosphere-Ionosphere System

Work was performed to generate and utilize simulations of the coupled solar-wind-magnetosphere-ionosphere system from the Integrated Space Weather Prediction Model (ISM) MHD code. Global MHD simulations of the magnetosphere are used to

examine the response of the coupled magnetosphere-ionosphere system to changes in the solar wind density. When a tangential discontinuity (TD) with a density increase contacts the bow shock, it results in a transmitted TD sandwiched between two oppositely traveling fast compression shocks. One of the fast compression shocks is transmitted into the magnetosheath ahead of the transmitted tangential discontinuity. The other fast compression shock travels upstream in the solar wind. The original density increase carried by the TD in the solar wind is split between the transmitted fast compression shock and the transmitted TD. The transmitted fast compression shock travels through the magnetosheath increasing the plasma density, magnetic field strength, and bulk flow speed. Immediately following the arrival of the fast compression shock at the magnetopause, the magnetopause begins moving earthward and a reflected fast compression wave is launched from the magnetopause upstream into the magnetosheath. The magnetopause continues to move earthward until it reaches its new pressure-balanced location. The upstream fast compression shock in the solar wind comes to rest at its final standoff location when the reflected fast compression wave from the magnetopause intercepts it. This interaction produces a second TD that travels through the magnetosheath back towards the magnetopause.

The merging rate at the dayside magnetopause increases during the interaction of the solar wind TD with the magnetosphere. The merging rate remains elevated from the moment that the initial fast compression wave reaches the magnetopause until the arrival of the second TD at the magnetopause. The length of this time interval is approximately 5-10 minutes. The transpolar potential in the ionosphere increases in response to the enhanced merging rate. Due to the inductive inertia of the coupled magnetosphere-ionosphere system, the transpolar potential responds slowly to the enhanced merging rate. The transpolar potential responds on time scales proportional to the instantaneous difference between the transpolar potential and the merging rate, the effective ionospheric Pedersen conductivity, and the region 1 current loop self-inductance. After the merging rate at the dayside magnetopause recovers to near original values, the transpolar potential decays slowly towards original values during an approximately 30-minute-long period. The transpolar potential remains elevated for a much longer interval the than the merging rate due to the inductive inertia of the coupled systems.

When a TD in the solar wind with a density decrease interacts with the magnetosphere, a similar series of phenomena occur. The result of the interaction is a transmitted TD sandwiched between two oppositely traveling fast shocks. A fast rarefaction shocks is transmitted into the magnetosheath ahead of the transmitted tangential discontinuity and a fast compression shock is launched upstream in the solar wind. The original density decrease carried by the TD in the solar wind is split between the transmitted fast rarefaction shock and the transmitted TD. The transmitted fast rarefaction shock travels through the magnetosheath decreasing the plasma density, magnetic field strength, and bulk flow speed. Immediately following the arrival of the fast rarefaction shock at the magnetopause, the magnetopause begins moving sunward and a reflected fast rarefaction wave is launched from the magnetopause upstream into the magnetosheath. The magnetopause continues to move sunward until it reaches its new pressure balanced location. The upstream fast compression shock in the solar wind comes to rest at its final standoff location when the reflected fast rarefaction wave from

the magnetopause intercepts it. This interaction produces a second TD that travels through the magnetosheath back towards the magnetopause.

The merging rate at the dayside magnetopause decreases during the interaction of the solar wind TD with the magnetosphere. After the merging rate at the dayside magnetopause recovers to near original values, the transpolar potential decays slowly towards original values. The transpolar potential remains diminished for a much longer duration than the merging rate due to the inductive inertia of the coupled systems.

4.4. Dayside Plasma Upflow Response to the Solar Wind

The high latitude auroral ionosphere supplies plasma to the magnetosphere. The first step in the chain of processes is the upwelling of ionospheric plasma in the topside ionosphere. The DMSP satellites are in an ideal position to observe this in the cusp/cleft region and dayside aurora. Figure 3 shows drift meter data (velocity parallel to **B**; up arrows indicate flow away from the Earth) from three consecutive passes of F13 superimposed on Polar/UVI images for the same times. ACE data showed a shock in the solar wind that arrived at the Earth at 0653 UT. Apparently, the cusp region upflow responded to the increased dynamic pressure.

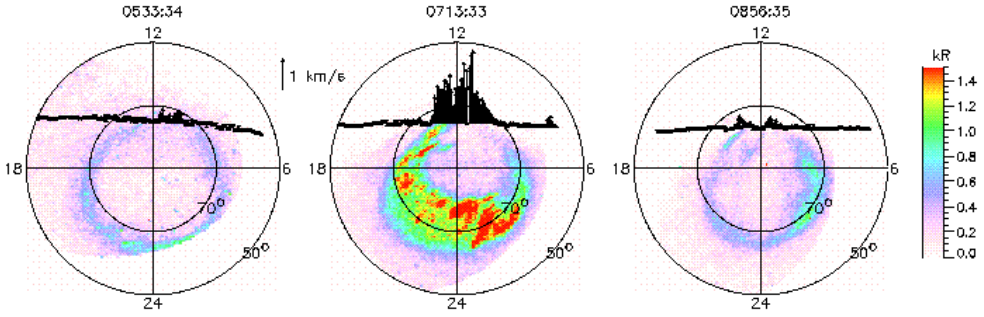

Figure 3. DMSP F13 drift meter data and Polar/UVI auroral images from 26 August 1998. A solar wind shock arrived at the Earth at 0653 UT.

We have examined enough events like this one so as to analyze statistically the relationship between the dayside upflows and the solar wind conditions. In this regard, we use the average value of the parallel velocity (Ave $V_{\parallel}$), the average parallel flux (Ave Flux), the fluence (average flux times the length of the upflow region), the length of the upflow region, and the flux weighted centroid of the upflow region in MLT. We compare these against several parameters from the solar wind: The y and z components of the IMF, the density (N) and velocity (V_x) of the solar wind, the dynamic pressure (Pd) and its variance (σPd), and the Kan-Lee electric field (Ekl). The solar wind quantities were averaged over the 40-minute interval preceding the upflow event. Table 1 shows the correlation coefficient between each upflow parameter and each solar wind parameter. Values in red indicate a confidence of interval ≥ 99%, blue 95% – 99%, and white < 95%. Clearly, the fluence is highly correlated with solar wind dynamic pressure while the average parallel velocity is highly correlated with the Kan-Lee electric field. Surprisingly, unlike the location of the cusp, the MLT centroid of these upflow regions is not highly correlated with IMF B_Y.

Table 1. Correlation of Upflows with Solar Wind Conditions							
	By	Bz	N	Vx	Pd	σPd	Ekl
Ave V‖	**0.56**	0.10	0.19	**0.71**	**0.68**	**0.70**	**0.81**
Ave Flux	0.10	-0.038	**0.51**	0.10	**0.63**	**0.52**	0.38
Fluence	**0.45**	0.18	**0.54**	0.31	**0.80**	**0.71**	**0.54**
length	**0.53**	0.36	0.32	**0.50**	**0.66**	**0.57**	**0.51**
MLT	0.24	-0.34	-0.01	0.22	0.062	0.14	0.36

4.5. ACE Magnetosphere-Ionosphere Interactions Study

Data from the Advanced Composition Explorer (ACE) satellite have been used to estimate the electromagnetic energy input from the magnetosphere into the ionosphere during magnetic storms and improve predictions of satellite drag. Estimates of the polar cap potential (Φ_{PC}) and dynamic pressure of the solar wind (P_{SW}) based on the Siscoe-Hill model, and of the electric field (E_{VS}) based on the Volland-Stern model using data from the magnetic field instrument (MFI) and the solar wind electron proton alpha monitor (SWEPAM) on ACE have shown promise as a predictive tool. Plots of the Sym-H and Dst indexes, DMSP equatorial plasma bubble (EPB) occurrence, $\Phi_{PC,}$ P_{SW}, and E_{VS} for all storms (56) with a minimum Dst ≤ –100 nT from January 1999 through June 2005 indicate that all three parameters, $\Phi_{PC,}$ P_{SW}, and $E_{VS,}$ show significant increases prior to storm onset. E_{VS} remains high throughout the main phase of each storm as the ring current is energized and Dst rapidly decreases to a minimum. There is generally a sharp decline in E_{VS} preceding the end of the storm's main phase and beginning of the recovery phase.

Of those 56 storms, seventeen were selected for further study based on pre-storm conditions and the availability of ACE data for the full storm interval. The data indicate very high correlations between Dst measurements and the quantity $I_{VS} = \int E_{VS}\, dt$ during the selected main phases with promising implications for satellite drag models and Dst prediction. A paper submitted to the Journal of Geophysical Research has been accepted for publication. A poster describing this work was also presented at the Space Weather Workshop in Boulder, Colorado, in April 2007.

5. VALIDATION OF THE WIDE BAND SCINTILLATION MODEL (WBMod)

In view of the importance of equatorial scintillation to GPS operations, a reliable predictive model is essential for mission planning and for post analysis. The benchmark scintillation model is the Wide Band model (WBMod). The name derives from the Wide Band Satellites, the data from which was used in the initial development of the model.

WBMod is a climatological model, giving the probability of scintillation as a function of geographic location, solar and geophysical parameters, and the time of night. The model has been used extensively for predictive purposes and has gone through many revisions incorporating new data sets since the initial release in 1980. The latest release,

Version 15, incorporates data taken over a ten-year period through the SCINDA network. This increases the overall data set in WBMod by about a factor of 2.

Our efforts in the past year have included studies to determine the feasibility of using GPS Scintillation measurements in the WBMod model.

5.1. Scintillation Effects on GPS

Equatorial scintillation is a phenomenon in which small-scale irregularities in the *F* region of the ionosphere interrupt radio communications between the Earth and orbiting satellites. The process occurs only at night and is limited to a region from the magnetic equator to about 20˚ to the North and South. The process results in large-scale scintillation bubbles which obliterate some regions of the sky to communication. The disruptions are greatest at low frequency and decrease in severity as frequency increases, but during solar moderate and maximum years, they are significant at the 1.5-GHz range at which the Global Positioning System operates. The end result, insofar as positioning with GPS is concerned, is loss of information from some or all satellites. It has been documented that under certain conditions, complete loss of GPS capability can result from scintillations. Therefore, equatorial scintillations are extremely important for systems that rely upon GPS, which, in this day and age, encompasses the better part of both civilian and military systems.

The Scintillation Network Decision Aid (SCINDA) is a nowcasting tool that provides a specification of the current scintillation conditions over a chosen theater. The system works like this. First, sensors placed at various strategic points around the globe monitor the power levels of signals from Earth-orbiting satellites. When scintillation along these links is detected, the measured scintillation intensity level is used along with empirical models of the scintillation bubble structure and evolution to generate regions of predicted communication outages which are then projected onto maps for chosen theatres. The current number of SCINDA stations at this writing is fourteen. Since the previous version of WBMod relied on only three stations in the equatorial region, it is clear that the addition of the SCINDA data constitutes a major improvement in WBMod reliability.

5.2. Scintillation and Frequency

There are two basic frequencies monitored by the SCINDA network. The first is the region around 250 MHz, which will be called the UHF here. This is monitored by listening to beacons from geostationary satellites using standard receivers. The second frequency monitored is around 1.5 GHz, which we will call the L-Band frequency. These data are obtained by NOVATEL single-frequency GPS receivers which have been specially modified to produce scintillation parameters. Both of these are used in the production of the SCINDA outage maps, although outage maps are currently produced only for the UHF. The GPS data are downshifted in frequency through an *ad hoc* algorithm to compliment the UHF data. There are, however, two stations that listen to fixed geostationary satellites at the L-Band. These are Ascension Island and Antofagasta. What is important, though, is that scintillation data from both systems is collected and archived continuously. It is therefore all available for incorporation into WBMod.

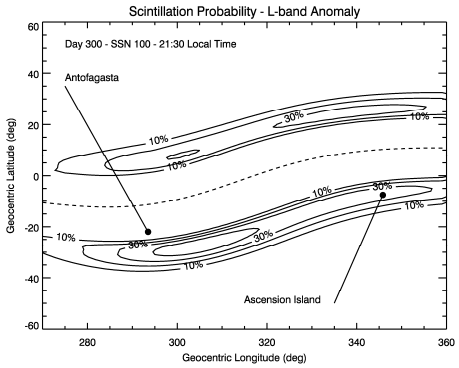

Figure 4. The probability of scintillation at the L-Band given by WBMod and shown as a function of geographic latitude and longitude for conditions near the maximum of L-Band scintillation. The peaks in the scintillation near the Appleton anomaly are evident. The dots show the two SCINDA stations for which fixed link L-Band scintillation data are available. The dashed line gives the magnetic equator.

The climatology of UHF and L-Band scintillation differ substantially. First, L-Band scintillation essentially goes away at solar minimum while UHF scintillation stays strong. Second, the UHF scintillation extends pretty much uniformly over the magnetic equator while the L-Band scintillation peaks at the Appleton anomaly crests at about 12˚ to 15˚ geomagnetic. This behavior is shown in Figure 4 for the Atlantic sector. Also of note is that the seasonal behavior of UHF and L-band scintillation are somewhat different. UHF scintillation persists pretty much unabated through the winter months while L-Band scintillation is much more peaked around the equinoxes.

So, L-Band scintillation is somewhat different from the UHF. As far as WBMod is concerned, though, there is no separate model for these two frequencies. Frequency bridging is continuous, of course, and is incorporated through a power law. It would seem to us that this portion of the model was developed with data from Ascension Island only. The significance of Figure 4 is that it shows strong L-Band scintillation at Ascension, but no scintillation at Antofagasta. In fact, the fixed link SCINDA data does show strong L-Band scintillation at Antofagasta, contrary to the model prediction.

It would appear, then, that Antofagasta L-Band data was not used in the construction of the latest version of WBMod, even the fixed link data to say nothing of the NOVATEL GPS. As for the other SCINDA station data, *none* of the NOVATEL results were used in developing the new model. Therefore, in spite of the fact that we now have a greatly improved WBMod at UHF frequency, the L-Band scintillation behavior appears to be wrong at Antofagasta. As for the rest of the world, save Ascension Island, the L-Band behavior of WBMod remains completely untested. The purpose of this study is to investigate the validity of the NOVATEL data and to see if it can be incorporated into WBMod in a future version.

5.3. Comparisons Between Fixed Link and NOVATEL Data

As a first step, we will compare the results from the fixed link (benchmark) and the NOVATEL GPS scintillation measurements in the context of what WBMod attempts to do. We chose the data for these comparisons from Ascension Island. This is where

L-Band scintillation is strongest and where the data set is most robust. We chose the fall of 2001 as a time period, which is near solar maximum.

The simplest thing we can do is to take a look at a single day, comparing the measurements from both the fixed link and from the GPS. Figure 5 shows one such day. In plotting the GPS, we have chosen to use the station-to-satellite link that exhibits the highest value of the scintillation index S_4, which is a measure of the signal power fluctuation. We see from this comparison that the scintillation structures being measured are essentially the same, with scintillation beginning about 21:00 UT and ending about one-half hour after UT midnight. The results from the GPS are smeared out to a greater extent than the fixed link because we have used the "hottest" satellite link. There is, therefore, a hand-off from one link to the other, resulting in more scintillating points overall. However, the GPS is certainly measuring the same structure.

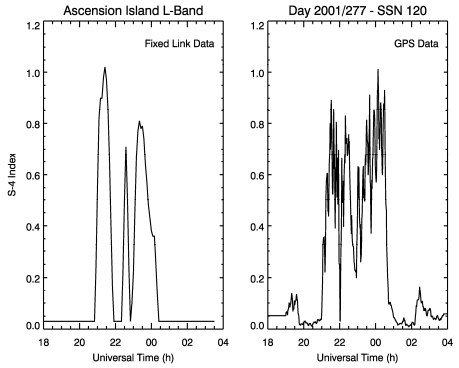

Figure 5. Line plots of the measured scintillation index taken from the Ascension Island fixed link (left) and from the "hottest" GPS link in the sky, for the same day in 2001.

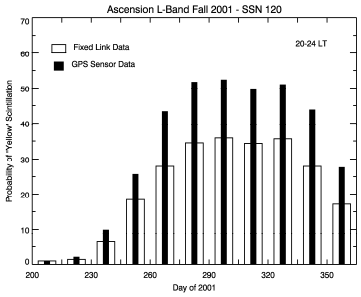

Figure 6. The seasonal behavior of scintillation at L-Band at Ascension Island, as measured by both the fixed link and by the GPS. The open histograms show the fixed link and the narrow ones the GPS.

The seasonal behavior is one of the most important characteristics of the scintillation to be monitored. Scintillation peaks around the equinoxes because, in order for large-scale bubbles to be formed, the magnetic field lines must be more or less perpendicular to the magnetic equator. This is because scintillation bubbles form shortly after sunset and both ends of the field line must be in darkness.

In Figure 6, we compare the season as measured by both the fixed link at Ascension and by the GPS sensors. The quantity plotted is the total probability of scintillation occurring during peak scintillation hours. We see, first, that the shape of the scintillation season is the same between the fixed link and the GPS. The GPS experiences more scintillation on average. This again is because we use as our metric the "hottest" GPS link in the sky. This means that there is more of a chance of the GPS following the scintillation structures as they move through the sky, as opposed to the fixed link which at Ascension looks approximately straight upward.

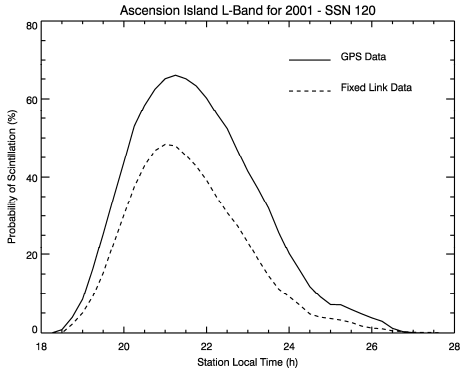

Figure 7. The local time behavior of scintillation at L-Band as registered by the fixed link and by the GPS at Ascension Island in the Fall of 2001.

A second issue in the comparison of the fixed link and the GPS is the behavior as a function of local time. In Figure 7, we show a comparison of the probability of scintillation as a function of the station local time. Again, we have used the "hottest" GPS link in the sky for the calculation. We see that the two curves peak at the same local time, that onset is the same at about 18:30 LT and that the scintillation dies away approximately one hour after local midnight. Again, the GPS result is somewhat larger because we have used the "hottest" link in the calculation.

So, we have seen that the NOVATEL GPS detect the scintillation in a way which is essentially the same as the fixed link, which *can* be used in WBMod modeling. This pertains to the day-to-day scintillation, to the seasonal and to the local time behavior. It would seem, then, that the use of the NOVATEL GPS data would be an essential element in improving the accuracy of WBMod at the L-Band. As we have seen, the data currently in WBMod at L-band is extremely limited, probably limited to a single station. We have also seen that WBMod is essentially incorrect in its prediction of scintillation at Antofagasta, so it seems clear that WBMod could use some improvement at GPS frequencies. So, just what is wrong with the NOVATEL data for WBMod use?

In order to understand why the NOVATEL data was not used in the creation of the latest WBMod, we must take a look at the details of how the modeling is carried out. The actual input to WBMod, which is a statistical model, is the distribution of the scintillation index S_4. Distributions of S_4 are created representing the data. Then, these model distributions are used to generate the two different quantities through which WBMod predicts scintillation, the probability of scintillation above a chosen S_4 level and the n-th percentile value of the S_4.

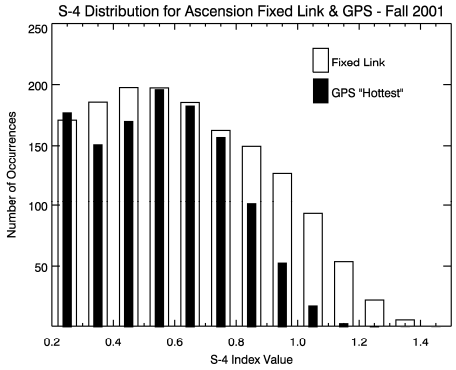

Figure 8. Histograms representing the distribution of the scintillation index S_4 during the peak scintillation period. The open histograms are for the fixed overhead link at Ascension Island and the filled histograms are the distribution of the "hottest" GPS link measurements.

So, we need to examine the distributions of S_4 from both the fixed link and the NOVATEL GPS. This is done in Figure 8 for the peak scintillation hours. We see clearly that, when viewed in this way, the behavior of the fixed link and the GPS do not match. Below an S_4 of about 0.8, the histograms correspond quite well. However, we see that the probability of scintillations above an S_4 of 0.8 as registered by the GPS is dramatically lower than our benchmark fixed link. At S_4 of unity, the GPS counts perhaps only 20% of the occurrences, as opposed to the fixed link.

It is little wonder, then, that a simple examination of the data would lead one to conclude that the NOVATEL GPS should not be used "as is" as input to the WBMod modeling process. The culprit, here, is dropout in the NOVATEL data. We have noted, in analyzing the data for SCINDA purposes, that a link will frequently be lost when the S_4 value exceeds 0.6 or so. Thus, the results of Figure 8 are not altogether surprising. It is interesting that the very effect of scintillation on the NOVATEL GPS receivers, dropout of a link, makes the data unusable for modeling that scintillation. Let us see if we can improve the situation, though.

5.4. A Case Study

Sometimes, looking at a single case can give one some direction on how to proceed. We have found a night during which the Ascension Island fixed link encounters a single scintillation bubble. During this night, activity is reported by the GPS both before and after the fixed link event.

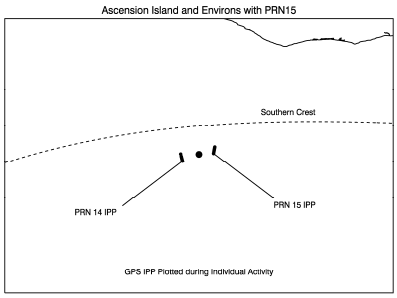

Figure 9. Ascension Island and environs on the day selected for the case study. The large dot gives the position of Ascension's fixed link. The smaller dots give the 300 km Ionospheric Penetration Points (IPP) of two GPS links on either side, during the times when these links showed scintillation activity.

Figure 9 shows the configuration of the Ascension fixed link and two GPS links on either side of the fixed link during the night selected for the case study. Since scintillation bubbles drift with the ionosphere from west to east, and since the two GPS links from PRN 14 and PRN 15 are at about the same magnetic latitude as the fixed link, we would expect that the scintillation bubble would be detected by all three links; first, by PRN 14, next, by the fixed link, then, by PRN 15 later in the night. We will be interested in what the data looks like during these three passes.

Let's begin by taking a look at the link to PRN 14. In view of the eastward drift of the scintillation bubbles, detection by PRN 14 will take place earlier than on the fixed link. Figure 10 shows the time series of measured S_4 for both PRN 14 and for the fixed overhead link.

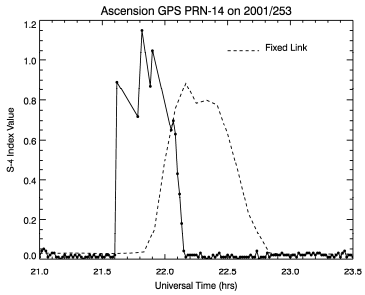

Figure 10. The scintillation index S_4 as measured by the NOVATEL GPS link to PRN 14 (solid line) and by the overhead fixed link at Ascension Island (dashed line). This day was chosen because there is only a single bubble in the region.

We see from Figure 10 that the link to PRN 14 does indeed drop out frequently. The cadence of the GPS and fixed link are different, with the GPS sampling once per minute, while the fixed link data comes every five minutes. We see, first of all, that the bubble shape has been more or less retained by the link to PRN 14. Were it the case that *all* S_4 values above a threshold dropped out, we would be at a loss to do much about the dropouts. However, we see that some of the strong S_4 values are registered by the GPS link. So, strong scintillation is retained at times by the NOVATEL unit. It's just that some of the strong scintillation points are missing. This suggests that interpolation of the NOVATEL data, PRN by PRN may bring the fixed link and GPS distributions in closer agreement.

We see that the structure of the scintillation bubble is basically retained by the NOVATEL GPS data, in spite of data dropouts, even at high S_4. It is interesting to estimate the velocity of the structure based on the detection time. We find that approximately 26 minutes elapse between the centers of the structure. From the map shown in Figure 9, we find that the NOVATEL link and the fixed link are separated by approximately 133 km. This leads to a drift velocity of 85 km/s, which is a very reasonable value for the drift of scintillation bubbles at this time of night.

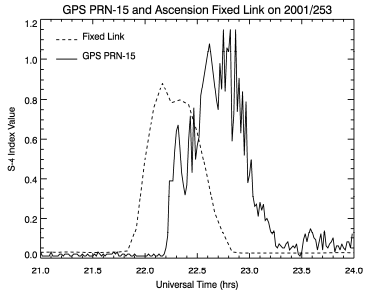

Figure 11. The scintillation bubble as detected by the fixed Ascension link (dashed line) and the NOVATEL link to PRN 15 to the east of the fixed link, on the same night as in Figure 7.

In Figure 11, we show the corresponding data for PRN 15, which we recall was situated to the east of the fixed overhead link at Ascension. Being to the east, the GPS link detects the bubble later in the night than those links to the west. The time separation is entirely due to bubble drift. As with PRN 15, we see that the bubble shape has been retained by the NOVATEL data. The bubble, as detected by PRN 15, is somewhat broader than that in the fixed link. This is entirely reasonable since the bubbles tend to spread out in longitude as they grow older.

We see something else significant in comparing Figure 10 and Figure 11. The data from PRN 15 shows substantially less dropout than did that from PRN 14. This seems reasonable if we consider that the scintillations tend to become weaker as the night wears on. It would seem that the dropout in the detection of bubbles early in the evening is more severe than in those detected later in the night. We should therefore take the local time into account in our comparisons.

5.5. Interpolating the NOVATEL GPS Data

We've seen that the structure of the scintillation bubbles is reproduced in the NOVATEL GPS data, in spite of data dropouts. This would suggest that the agreement between the fixed link and the GPS S4 distributions can be improved by replacing the dropouts with interpolated values. To try to reproduce the fixed link distributions at Ascension, we select NOVATEL points within 5˚ of the station latitude. This is to avoid complications due to the variation of the scintillation with latitude. So, we restrict the NOVATEL data to the vicinity of the fixed link. We also restrict the NOVATEL data to links above 30˚ in elevation. This is to avoid multi-path effects which contaminate the GPS data at low elevations.

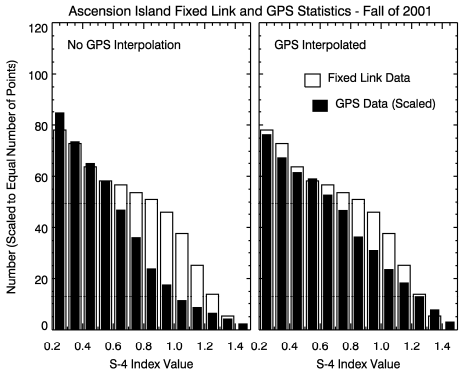

Figure 12. A comparison of the fixed link and GPS distribution of the scintillation index S_4. The left panel shows the result without interpolation of the NOVATEL data through data dropouts and the right uses interpolation. The local time range is 21:00 to 22:00 LT, the peak time of scintillation.

The prescription is really quite simple. We take all the NOVATEL data within range, we separate it PRN by PRN into a time series, then, we interpolate linearly between any missing points. Figure 12 compares the results for the peak hour of scintillation. We see that interpolation has improved things considerably. Aside from a slight shoulder in the fixed link data, the fixed link and the GPS S_4 distributions compare very favorably. At least the results are much better at high S_4 with the interpolation. However, it would seem that we are still missing some of the S4 around the 0.8 to 1.1 range. This may be due to the fact that very narrow structures are missed entirely.

We saw, before, in our case study, that the dropouts were more severe at earlier local times than at later local times. We, next, take a look at the 20:00 to 21:00 LT sector, the time when scintillation begins. These results are shown in Figure 13, both with and without the interpolation. Here, we see that the results prior to interpolation are more severely deficient.

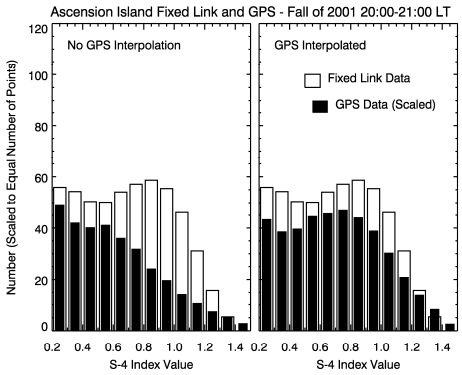

Figure 13. A comparison of the fixed link and GPS S_4 distributions at early local time, when the scintillation is just getting started. The left shows the comparison without GPS interpolation and the right panel shows the interpolated result.

The right panel of Figure 13 shows that interpolation has retrieved the majority of the high S_4 values. The difference between the early and later local time case is that at early local time, the entire GPS distribution with interpolation is low by perhaps 20%.

This, again, must mean that we are missing some structures altogether. This is not surprising if the structures are narrow and the dropout is severe.

5.6. NOVATEL Scintillation Summary

We have seen that the wealth of NOVATEL GPS data collected by the SCINDA accurately reflects the seasonal and local time behavior at GPS frequency, as evidenced by comparing the fixed link data to the GPS at Ascension Island during solar maximum. The NOVATEL data is deficient for direct use in modeling by WBMod, however, because of data dropouts at high S_4. A case study showed us that the bubbles are still represented reasonably well through the data dropouts, so that the distributions of S_4 might be improved upon by interpolation through the data dropouts.

Simple interpolation PRN by PRN has been shown to indeed improve the agreement between the fixed link and the GPS distributions. The question, then, is whether the interpolated distributions are now adequate for modeling. In light of the fact that WBMod at GPS frequencies is virtually untested outside of the region of Ascension Island, it would seem to us that incorporation of the interpolated distributions into the model would be an important improvement. We suggest that this be considered in an updated version of WBMod.

An informative companion study could also be done to assess the soundness of the current version of WBMod. In determining that WBMod Version 15 was deficient for Antofagasta, predicting no GPS frequency scintillation when, in fact, a substantial amount was measured, we used the fixed link data at Antofagasta. Instead, we could do a similar comparison using the "hottest" GPS link and do so for all the 14 SCINDA stations with NOVATEL data available. This would seem to be an important piece of work for addressing the worldwide validity of WBMod for GPS frequencies.

PUBLISHED PAPERS

Burke, W. J., Penetration Electric Fields: A Volland-Stern Approach, *J. Atmos. Solar-Terr. Phys.*, (in press) 2007.

Burke, W. J., **L. C. Gentile** and C. Y. Huang, (2007), Penetration Electric Fields Driving Main-Phase Dst, *J. Geophys. Res.*, 112,A07208, doi:10.1029/2006JA012137.

Burke, W.J., C. Y. Huang, F. A. Marcos and J. O. Wise, Interplanetary Control of Thermospheric Densities during Large Magnetic Storms., *J. Atmos. Solar-Terr. Phys., 69*, 279, 2007.

Decker, D.T. and **L.F. McNamara**, (2007), Validation of Ionospheric Weather Predicted by Global Assimilation of Ionospheric Measurements (GAIM) Models, *Radio Sci.*, 42, RS4017, doi:10.1029/2007RS003632.

Lin, C. S., H.-C. Yeh, B. R. Sandel, J. Goldstein, F. J. Rich, **W. J. Burke**, and J. C. Foster, Convection Plasma Drifts in the Inner Magnetosphere Associated with a Plasmaspheric Drainage Plume, *J. Geophys. Res.*, 112, A05216, doi:10.1029/2006JA011819, 2007.

Maynard, N. C., **W. J. Burke**, Y. Ebihara, **D. M. Ober**, G. R. Wilson, J. D. Winningham, A. Balogh, C. J. Farrugia, H. J. Singer, M. Ejiri, A. Fazakerley, H. Réme, and M. Andre, Characteristics of merging at the magnetopause inferred from dayside 557.7-nm all-sky images: IMF drivers of poleward moving auroral forms, *Annal. Geophys., 24*, 3071, 2006.

McNamara, L.F., D.L. Cooke, C.E. Valladares, and B.W. Reinisch, Comparison of CHAMP and Digisonde plasma frequencies at Jicamarca, Peru, *Radio Sci.,* Vol. 42, RS2005, doi:10.1029/2006RS003491, 2007.

McNamara, L.F., D.T. Decker, J.A. Welsh and D.G. Cole, (2007), Validation of the Utah State University Global Assimilation of Ionospheric Measurements (GAIM) model predictions of the maximum usable frequency for a 3000 km circuit, *Radio Sci.*, 42, RS3015, doi:10.1029/RS003589, 2007.

Mishin, E. V., F. A. Marcos, **W. J. Burke**, D. L. Cooke, C. Roth, and V. P. Petrov, (2007), Prompt thermospheric response to the 6 November 2001 magnetic storm, *J. Geophys. Res.*, 112, A05313, doi:10.1029/2006JA011783, 2007.

Ober, D. M., N. C. Maynard, **W. J. Burke**, K. D. Siebert, C. T. Russell, J. D. Scudder, and H. J. Singer, "Shoulders" on the High-Latitude Magnetopause: Polar/GOES Observations, *Geophys. Res. Lett*., *33*, L04196, doi:10 1029/2005GL024655, 2007.

Pradipta R., A. Labno, M. C. Lee, **W. J. Burke**, M. P. Sulzer, J. A. Cohen, L. M. Burton, S. P. Kuo, D. L. Rokusek, (2007), Electron precipitation from the inner radiation belt above Arecibo, *Geophys. Res. Lett.,* 34, L08101, doi:10.1029/2007GL029807.

Rich, F. J., J. M. Bono, **W. J. Burke, and L. C. Gentile,** (2007), A Proxy for the Dst index, *J. Geophys. Res*., 112*,* A05211, doi:10.1029/2005JA011586.

PRESENTATIONS

There were numerous informal presentations on the Calibration and Validation Efforts, the GAIM Model Validations and Magnetosphere-Ionosphere Coupling. The following describes the presentations at formal conferences.

Burke, W. J. , C. Y. Huang, and F. J. Rich, Magnetosphere-Ionosphere Coupling in the Main Phase of Magnetic Superstorms, *Chapman Conference on Mid-Latitude Ionospheric Dynamics and Disturbance*s, invited presentation, Yosemite National Park, 1 - 6 January 2007.

P.H. Doherty was an invited speaker at the Space Weather Workshop in Boulder, CO. The title of her presentation was "WAAS Response to the Space Weather Events of 2003-2006 and Preparations for Solar Maximum."

L. C. Gentile presented a poster entitled "Predicting Stormtime Equatorial Plasma Bubbles" by L.C. Gentile, **W.J. Burke** and C.Y. Huang at the Space Weather Workshop in Boulder, CO.

L.F. McNamara presented "Validation of the Utah State University Global Assimilation of Ionospheric Measurements (GAIM) Model" at the AGU Meeting in Acapulco, Mexico, in May 2007.